Innovaciencia ISSN: 2346-075X Bucaramanga - Colombia

Original Research and Innovation Article

Innovaciencia 2026; 14 (1): e5819

Effect of Micropatterning of Metallic Surfaces on Nucleate Pool Boiling

Efecto de la microestructuración de superficies metálicas sobre la ebullición nucleada en piscina

Omar Sinhue Delgado-Ramírez [1*], Héctor Javier Vergara-Hernández [1] , Octavio Vázquez-Gómez [1], Gerardo Marx Chávez-Campos [1]

How to cite this article: Delgado-Ramírez OS, Vergara-Hernández HJ, Vázquez-Gómez O, Chávez-Campos GM. Effect of micropatterning of metallic surfaces on nucleate pool boiling. Innovaciencia. 2026;14(1):e5819.

https://doi.org/10.15649/2346075X.5819

Received: 16 October 2025
Accepted: 11 June 2026
Published: 17 June 2026

Highlights:

- Micropatterned surfaces reduced bubble diameter by up to 32% during nucleate boiling.
- Surface micropatterning increased nucleation site density by approximately threefold.
- Square micropatterns achieved the highest heat transfer coefficient (11.45 W cm^{-2} K^{-1}).

[1] Tecnológico Nacional de México - Instituto Tecnológico de Morelia CP 58120, División de Estudios de Posgrado en Investigación, Doctorado en Ciencias de la Ingeniería, Morelia, Michoacán, México. * Corresponding author omarsinhued@gmail.com

Innovaciencia ISSN: 2346-075X Bucaramanga - Colombia

Original Research and Innovation Article

ABSTRACT

Introduction. Nucleate boiling occurs when the surface temperature exceeds the liquid's saturation temperature, leading to vapor bubble formation. Surface roughness strongly affects bubble nucleation and dynamics, thereby enhancing heat transfer efficiency during nucleate boiling. **Objectives**. To characterize bubble nucleation, growth, and detachment during pool nucleate boiling using two micropatterned surfaces: 1) a vertical-patterned surface (VPS) and 2) a square-patterned surface (SPS), and to compare their performance with that of a smooth surface (SS). **Materials and Methods.** An acrylic container was fixed to metal surfaces to study the liquid pool. A novel methodology employing the Peltier effect allows the control of the process variables and ensures reproducibility. Bubble dynamics were captured with a high-speed camera, while thermal responses were monitored by thermocouples in the liquid and on the metal surface. **Results.** Micropatterned surfaces decreased bubble diameter by 32%, and increased nucleation sites threefold compared to smooth surfaces. The highest convection coefficient was observed for the square surface (11.45 $Wcm^{-2} K^{-1}$) followed by the vertical (7.7 $Wcm^{-2} K^{-1}$), and smooth (5.4 $Wcm^{-2} K^{-1}$) surfaces, these values are unusual in the literature, since the study was carried out at the micrometric level, suggesting a significant analysis for microscale cooling applications. **Conclusions.** A roughness defined by micropatterning allows control over nucleate boiling and improves heat dissipation in applications that require high power density, such as next-generation electronic devices and aerospace technologies.

Key words: Aluminum Alloy; Heat Transfer; Micro-Patterned; Pool Boiling.

RESUMEN

Introducción. La ebullición nucleada ocurre cuando la temperatura superficial supera la temperatura de saturación del líquido, generando burbujas de vapor. La rugosidad superficial influye significativamente en la nucleación y dinámica de las burbujas, mejorando la eficiencia de la transferencia de calor durante la ebullición nucleada. **Objetivos.** Caracterizar la nucleación, el crecimiento y el desprendimiento de burbujas durante la ebullición nucleada en piscina utilizando dos superficies micropatronadas: 1) una superficie con patrón vertical (VPS) y 2) una superficie con patrón cuadrado (SPS), y comparar su desempeño con el de una superficie lisa (SS). **Materiales y Métodos.** Se fijó un recipiente acrílico a superficies metálicas para estudiar la ebullición en piscina. Una novedosa metodología basada en el efecto Peltier permitió controlar las variables del proceso y asegurar la reproducibilidad de la experimentación. La dinámica de las burbujas se registró mediante una cámara de alta velocidad, mientras que las respuestas térmicas se monitorearon con termopares ubicados en el líquido y en la superficie metálica. **Resultados.** Las superficies microestructuradas redujeron el diámetro de las burbujas en un 32 % e incrementaron tres veces los sitios de nucleación en comparación con las superficies lisas. El mayor coeficiente de convección se obtuvo en la superficie con estructura cuadrada (11,45 $Wcm^{-2}K^{-1}$), seguida de la superficie con estructura vertical (7,7 $Wcm^{-2}K^{-1}$) y la superficie lisa (5,4 $Wcm^{-2}K^{-1}$). Estos valores son poco comunes en la literatura, ya que el estudio se realizó a escala micrométrica, lo que sugiere un análisis relevante para aplicaciones de refrigeración a microescala. **Conclusiones.** Una rugosidad superficial definida mediante microestructuración permite controlar la ebullición nucleada y mejorar la disipación de calor en aplicaciones que requieren alta densidad de potencia, como dispositivos electrónicos de nueva generación y tecnologías aeroespaciales.
Palabras clave: Aleación de aluminio; transferencia de calor; microestructuración de superficies; ebullición en piscina.

Palabras clave: Aleación de aluminio; transferencia de calor; superficies microestructuradas; ebullición en piscina.

INTRODUCTION

Nucleate boiling is a very effective heat transfer mechanism due to the large amount of heat absorbed by the liquid medium during the phase change from liquid to gas. Phase change processes are widely used in the nuclear industry, aerospace, metallurgy, and other engineering areas. However, it´s a complex phenomenon to study, since it involves heat and mass transfer, phase change, and multiphase flow, which makes it difficult to analyze and carry out the experimentation. Several factors influence heat transfer during nucleate boiling: nucleation sites, active nucleate diameter, frequency of bubble detachment, and bubble contact angle; these characteristics directly influence the temperature distribution of the wall surface [(1-4)].

The bubble separation process and the bubble detachment diameter are the most important parameters in heat transfer analysis. Several experimental studies on bubble dynamics during nucleate boiling have investigated the processes of nucleation, growth, and variations in the contact angle. Researchers have focused on the influence of surface tension, buoyancy and drag forces, which determine the detachment of bubbles from the heated surface. From these investigations, numerous correlations have been established to describe the relationship between bubble detachment diameter and the frequency of bubble release [(5-8)]. Another important factor that has been reported in the literature is the effect of the surface roughness. The roughness of the surface has a significant impact on fluid flow behavior and heat transfer. It has been observed that, as the surface roughness increases, the number of active nucleation sites increase and the contact angle diminishes, while the vorticity increases which favors the frequency of detachment and, therefore, the surface heat flux [(9-10)]. Other researchers have investigated the effect of the type of fluid on nucleate boiling.

The diameter of the bubble at the time of detachment, the frequency of bubble exit, and the density of the active nucleation site have been studied by combining the effects of heat flux variation and roughness. The results are compared with the predictions of existing models of bubble nucleation behavior in literature. It is suggested that new correlations of bubble nucleation are established, that incorporate the important effect of surface roughness, so that the new correlations can be applied to a wide range of surfaces during the nucleate boiling [(11)].

On the other hand, recent studies have focused on the effect of micro-electronic refrigerant systems, making micro-milling and lithography [(12)] to increase the heat dissipation of micro-electronic refrigerant systems and to favor uniform heat transfer [(13-16)]. Nucleate boiling phenomena have not only been studied experimentally, but numerical simulation has been a good tool to model the boiling of nucleated pools from multiple nucleation sites at different boiling water regimes, ranging from discrete bubbles to area steam. The method is based on interface tracking in which the liquid-vapor interface is resolved using computational fluid dynamics (CFD). Conjugated heat transfer between the wall and the fluid is included to adequately capture the temperature field and demonstrate the bubble growth process ([17-19]. Various authors have characterized nucleated boiling employing electrical resistances as a heating source [20-21], demonstrating that a non-uniform electric field is related to the dynamic behavior of the bubbles; it´s essential to avoid the electrical inertia that is generated in specific electrical devices using a Peltier cell that allows control over the heating of the surface and promotes the study of bubble generation.

This study presents a novel contribution to the understanding of nucleate boiling on metallic surfaces by demonstrating new micropatterning designs that enhance heat transfer through an increased number of nucleation sites and a higher bubble detachment frequency. The use of a Peltier cell as a heat source further improves the methodology by eliminating thermal inertia typically associated with electrical resistors, enabling more precise temperature measurements during the experimental process. Overall, this innovation highlights the relevance of micropatterned surfaces as efficient heat sinks, offering valuable insights for future applications in advanced cooling systems and high-power electronic devices.

MATERIALS AND METHODS

The experimental study, and the process of analyzing nucleate boiling on micropatterned surfaces is illustrated in (**Figure 1)**. It began with the preparation of surfaces through electronic design and the printing of metallic patterns. If the micropatterning was not correct, the printing was repeated. Once the micropatterning was adequate, the roughness of the printed surface was measured, and the experimental procedure advanced. During the experiments, a power supply provided voltage to the Peltier cell, while thermocouples monitored the temperature. Bubble dynamics were recorded using a high-speed camera. Finally, the acquired data were analyzed, revealing the thermal history, bubble dynamics through photographs, and bubble detachment frequency.

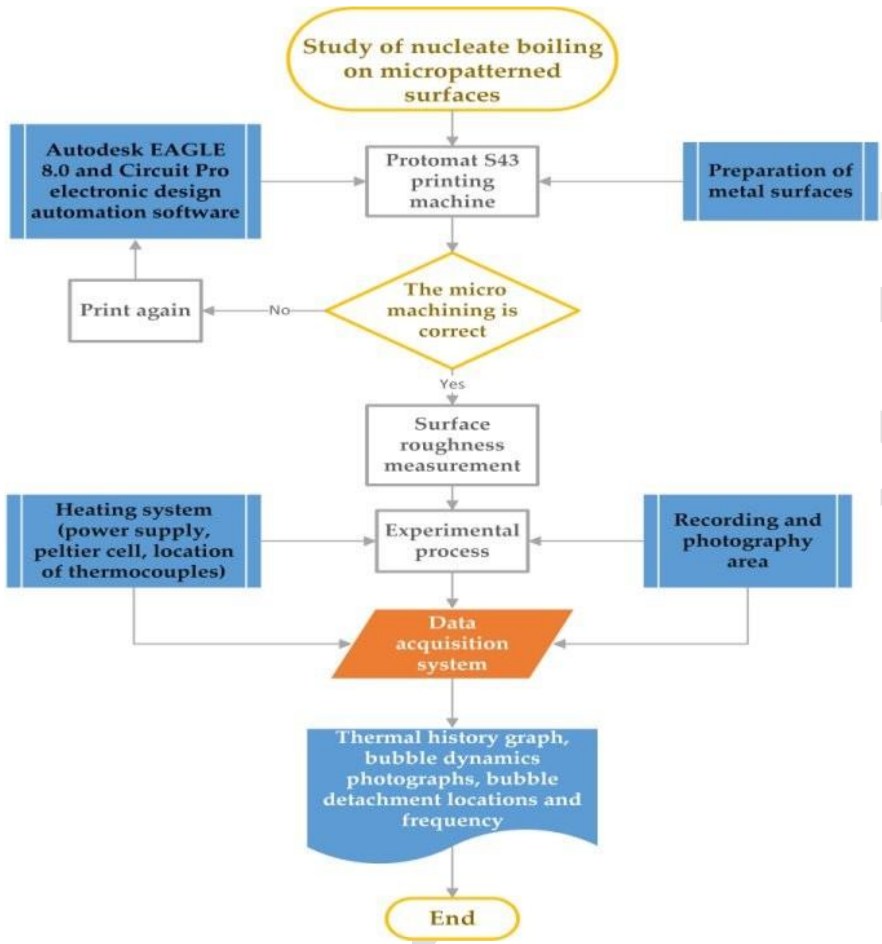

Figure 1. Flowchart of the phases and procedures of the investigation.

The surface micro-milled patterns used in this study (**Figure 2**) were designed to promote early nucleation and increase nucleation sites; they were fabricated using the electronic design automation software Autodesk EAGLE 8.0 for printed circuit boards (PCB). Before micro- milling, 300 mm^2 square sections (sheet caliber 26) were cut. According to the type of micro- milling pattern on the surface exposed to the cooling medium, the sheets were classified as a). smooth surface (**SS**), b). vertical pattern surface (**VPS**), and c). square pattern surface (**SPS**).

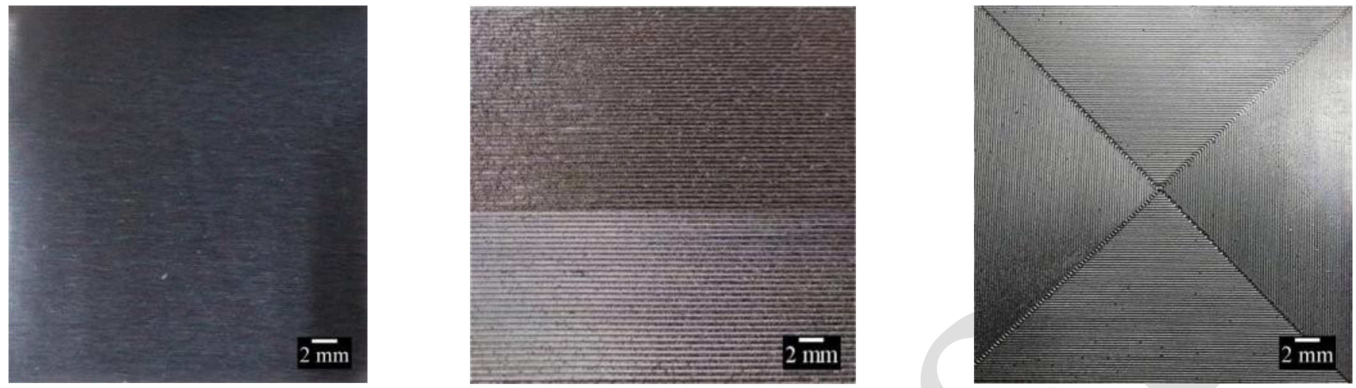

a). **b).** **c).**

Figure 2. Photographs of the sheet for the type of surface pattern: **a).** SS, **b).** VPS, and **c).** SPS. The images correspond to the full sheet area.

The preparation of each sheet consisted of polishing it with 1 μm alumina powder, followed by mounting them in a Proto Mat S43 printing machine to carry out micro-milling using CIRCUIT PRO software. A 100 μm tungsten carbide drill bit was used to produce the SPS and VPS surfaces with a separation between channels of 200 μm, giving a total of 150 channels, **Figure 3**. Light grinding was carried out on the SS sheet to ensure that the three sheets had the same thickness with the peaks of the micro-milling surfaces above the plane of the top of the SS sheet. **Table 1** shows the surface area, volume, and area scaling factor (the ratio of the exposed area to the projected area, i.e., that of the SS sheet for each one of the micro-milled surfaces).

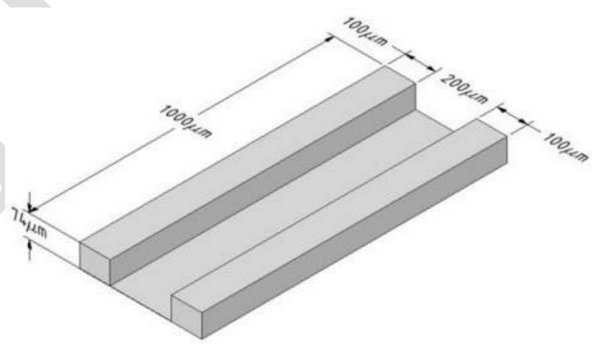

Figure 3. Details of the geometry of the micro-milled surfaces VPS and SPS.

Table 1. Surface area, volume, and area scaling factor for each of the surfaces

Surface Type	Area m^2	Volume m^3	Area Scaling Factor
SS	9×10^{-4}	4.14×10^{-7}	1
VPS	1.4×10^{-3}	6.2×10^{-7}	1.55
SPS	2.5×10^{-3}	9.65×10^{-7}	2.74

The micro-milling operation generated roughness in the channel groove and small-scale burr on the peaks. To characterize the roughness level, a surface roughness tester SR200 was used, controlled by the Surface Pressure Enterprise software. The roughness tester has a plunger on its lower surface, with a needle to register undulations on the surface; the plunger displacement was fixed at 1 mm. The average roughness of the micro-milled surfaces is shown in **Table 2**. As can be seen, it is much larger than that of the smooth surface.

Table 2. Average surface roughness

Surface Type	Average roughness (µm)
SS	1.89
VPS	75.86
SPS	74.16

Data Availability

The dataset supporting the findings of this study has been deposited on Mendeley Data and is publicly available under the title: Delgado Ramirez, Omar Sinhue; Vergara Hernández, Héctor Javier; Vázquez Gómez, Octavio; Chávez Campos, Gerardo Marx (2026) "Study of Heat Transfer on Micropatterning Surfaces. Supplementary Data", Mendeley Data, V2, doi: https://doi.org/10.17632/dtc8ts84td.2

Experimental setup.

The main components of the experimental setup (**Figure 4**) are 1) an AC power source, 2) a temperature measurement probe arrangement (type-K thermocouples), 3) a data acquisition system, 4) a high-speed camera, 5) Peltier cell and 6) liquid pool.

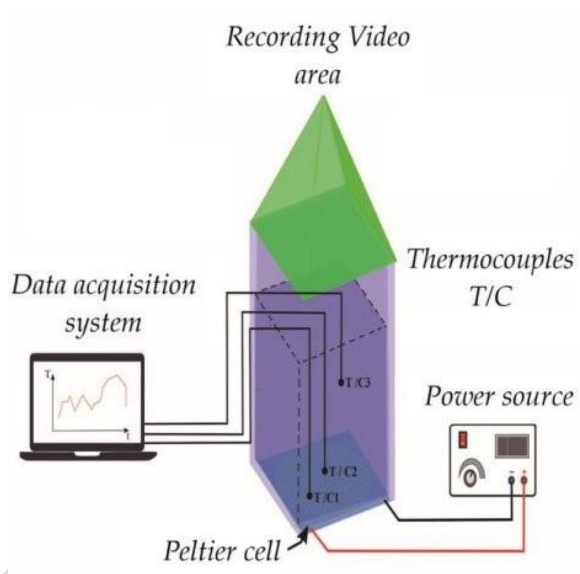

Figure 4. Experimental set-up: **1).** AC power source, **2).** Thermocouples, **3).** Laptop, **4).** High speed camera, **5).** Peltier cell and **6).** Liquid pool.

To contain the cooling medium, a 30 mm x 30 mm x 80 mm plexiglass container was built and mounted on each of the sheets using high-temperature silicon. The cooling medium was 1.5 10^{-5} m^3 deionized water. On the bottom surface of the sheet, a thin film of silver-based thermal paste Halnziye Hy710 was to attach the Peltier cell; the thermal paste was used due to its thermal conductivity which allows transferring the thermal energy from the Peltier cell without heat loss. The Peltier cell provides a constant heat flow that keeps the fluid in a state of permanent boiling, in addition to maintaining a controlled low temperature according to the operating conditions, with the use of the Peltier cell, thermal inertia is avoided, which is a phenomenon characteristic of an electrical resistance heating system. The cell was operated at 9 V, the surface temperature of the sheets was measured during the experimentation by a thermocouple type-K in direct contact with its hot face with the fluid, thermocouples labeled as "T/C 1" and "T/C 2" were welded, and a thermocouple "T/C 3" was used to measure the evolution of the temperature in the liquid sinus, located in the middle part of the liquid pool (1/2). The positions of the thermocouples are indicated in the elevation diagram in (**Figure 5**). Bubble nucleation and growth were characterized through video recordings with a Canon T7 high-speed camera with an 18-55 mm focal length at a frame rate of 200 frames per second and a resolution of 24.1 pixels/micron. The thermal response of each thermocouple was acquired with a Temp Scan/1100 Iotech data acquisition card at a frequency of 1 Hz, controlled with the software ChartView 1.02.

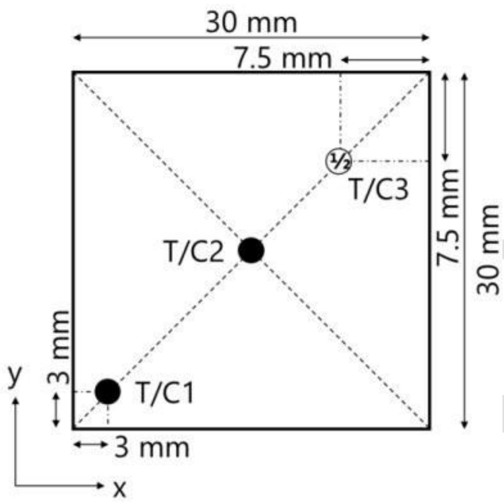

Figure 5. Position of thermocouples inside of the liquid pool.

Thermal Model

The heat transmitted to the pool liquid was estimated to be a mathematical model based on a heat energy balance. Figure 6 shows a schematic representation of the experimental setup. The Peltier cell is made up of the union of two semiconductor materials, one that absorbs (hot surface) and the other that releases (cold surface) the heat generated by the passage of current, thus, generating a temperature difference between its sides; the heat then flows into the liquid pool through the silver paste and the aluminum alloy sheet. It was assumed that the Peltier cell operates under steady-state conditions so that the heat flow is practically unidirectional towards the hot surface of the cell that is in indirect contact with the aluminum foil through the thermal paste.

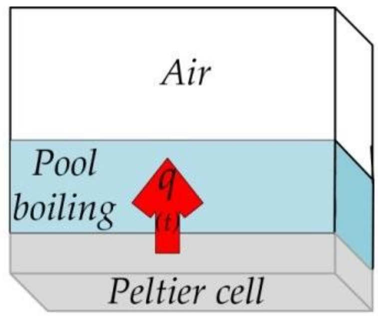

Figure 6. Schematic representation of the experimental setup for the development of the mathematical model. The arrows indicate the heat flow through the system.

From the general energy balance equation, it is established that:

$$\cancel{E_{in}} + E_{gen} - E_{out} = E_{acc} \qquad (1)$$

The energy generated in the system is due to the electrical power of the Peltier cell, the voltage remained constant in all cases (9 volts) and the amperage varies depending on the type of surface and as a function of time (2 to 3 Amperes), until the system reaches a steady state, this electrical power is lost in the system due to the flow of heat that is delivered by natural convection between the surface and the fluid and the energy accumulated in the fluid inside the pool, developing the eq. (1) in a function of the operating parameters in the experimental system is:

$$V * I = h * A_s(T_s - T_m) + \rho * C_p * V_m \frac{(T_m - T_\alpha)}{\Delta t} \qquad (2)$$

Where;

V = voltage delivered by the Peltier cell (volts); I = amperage delivered by the Peltier cell (amps); As = area as a function of surface exposed to heat transfer (m^2);Ts = temperature of the sheet average value of thermocouples T/C1 y T/C2 (K); Tm = temperature of the medium (water), T/C3 (K);ϱ = density of water as a function of temperature (kg m^{-3});Cp = specific heat of water as a function of temperature (J K^{-1} kg_{-1}); Vm = volume of water contained in the pool ($1.5x10^{-4}$ m^3); Tα = surrounding air temperature (298 K); Δt = time differential (s); h = unknown convection coefficient of the system to be solved (W/cm^2 K)

The accumulated energy was calculated using the thermal response recorded by the T3 thermocouple (**Figure 5**) and direct finite differences. It should be noted that the macroscopic energy balance presented above does not calculate the heat removed by the bubbles formed during heating, it only considers the surface heat flux removed into the pool of liquid.

The amount of heat extracted from the liquid volume is significantly greater than the energy required for bubble formation. The surface tension of water contributes an energy in the order of microjoules per bubble, which is negligible compared to the latent heat of vaporization. On micromachined surfaces, where more bubbles are generated, the additional energy associated with surface tension remains positive, but minimal, slightly reducing the net heat extraction without altering the heat transfer conditions. Since the pool boiling analysis already accounts for the energy exchange from the liquid volume, omitting this term does not significantly affect the estimated heat transfer coefficients.

RESULTS

Thermal Response

The results shown in sections 3.1-3.3 are triplicate data from the experiments and are intended to measure the reliability and repeatability of the tests performed depending on the surface type. The thermal responses measured on the sheet surface and in the liquid core are presented in **Figures 7a** and **b**, respectively. The reproducibility of the experiments is better on the micropatterned surfaces than the smooth surface by the error shown. This difference is attributed to the fact that the micro-milling surfaces present better homogeneity concerning the bubble nucleation sites due to micropatterned and better control over boiling. On the other hand, the reproducibility in the measurement of the temperature of the liquid sine presents a more significant error in the temperature of the smooth surface of around 2 K when reaching the stable state. However, the reproducibility of the experiments is acceptable since the error can be attributed to the constant agitation of the medium by boiling.

Innovaciencia
ISSN: 2346-075X Bucaramanga - Colombia
Original Research and Innovation Article

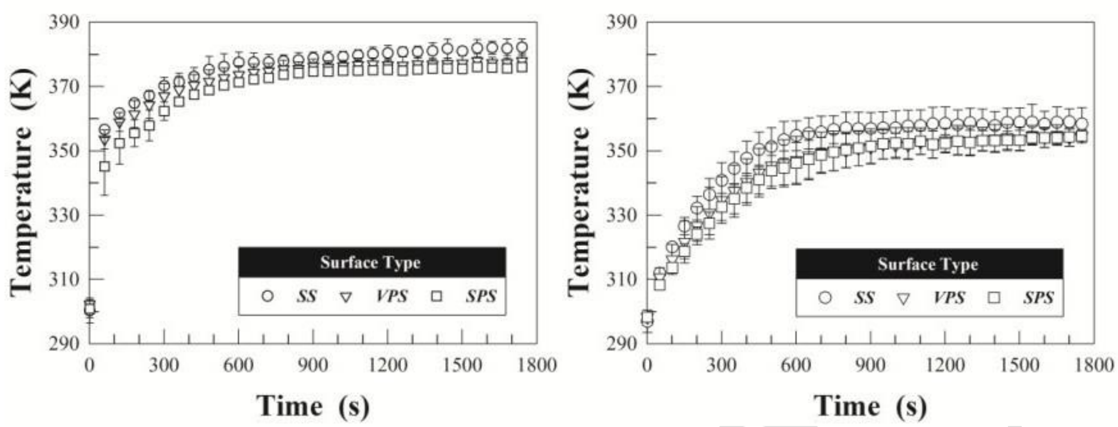

a) b)

Figure 7. Effect of surface type on the thermal response **a).** on the surface of the sheets**. b).** in the liquid pool.

According to **Figure 7a**, the fluid in the vicinity of the SS surface reaches a maximum average temperature of 384 K. In comparison, the micro-milled surfaces reach maximum temperatures of 380 and 377 K for the VPS and SPS surfaces, respectively. Furthermore, before reaching the steady state, the heating rate of the SS surface is about 3 K min^{-1}, which is slightly higher than that of the other micro-milled surfaces of 2.7 and 2.5 K min^{-1} for the VPS surfaces and SPS, respectively. The steady state for the thermal response in the fluid is shown in **Figure 7b**, the SS surface reaches an average temperature of 360 K (1060 s), while for the VPS and SPS surfaces, 357 K (960 s) and 355 K (at 880 s), respectively.

Bubble Dynamics

Bubble formation and growth were tracked for 1800 s. **Figure 8** shows the bubble characteristics at different times (5, 15, and 30 min) during the experiments as a function of surface type. Bubble growth on the SS surface is illustrated in (**Figures 8 ac**). A very limited number of bubbles (approximately 28) are formed during the experimental run. Bubble growth is gradual, reaching an average bubble diameter of ~3.3 mm after 30 minutes which was the largest among the surfaces studied. From the images it is evident that the number of bubbles quickly reaches a steady state condition, i.e., the nucleation rate after the first bubbles were formed is null or very low. From the results it is inferred that the flow towards the liquid/solid interface of the smooth type of surface is obstructed by the low rate of bubble detachment, making it difficult for new bubbles to form and, therefore, making it difficult to extract heat from through the formation of bubbles, so it is inefficient.

The behavior of the bubbles formed on the vertical micromachined surface can be observed in (**Figures 8d-f**). The behavior of the surface has a null presence of bubbles until minute 5, after this time there is the formation of a few nucleation sites which are mostly present in the center of the surface, however, there are areas without generation of bubbles. The bubbles compared to the smooth surface; the bubbles have a smaller diameter because the bubble grows very slowly and there is a greater number of active nuclei (66 nucleation sites). Bubble growth is gradual reaching an average size of ~2.63 mm after 30 min. The generation of new nucleation sites is maintained for up to 15 min, after which time the sites remain constant.

Bubble dynamics on an SPS surface are shown in (**Figures 8 g-i**). This type of surface produced the largest number of bubbles, covering the heat transfer area almost completely, the geometrical pattern of the surface favors earlier nucleation and a larger number of active nucleation sites (81 nucleation sites on 9 cm^2 of micro-milled surface), and smaller bubble diameters, concerning the VPS surface. The SPS surface produces a nearly constant nucleation rate: the bubble population and size distribution at 5, 15, and 30 minutes is similar, showing only a slight increase, both in the number of bubbles and their size at 30 minutes.

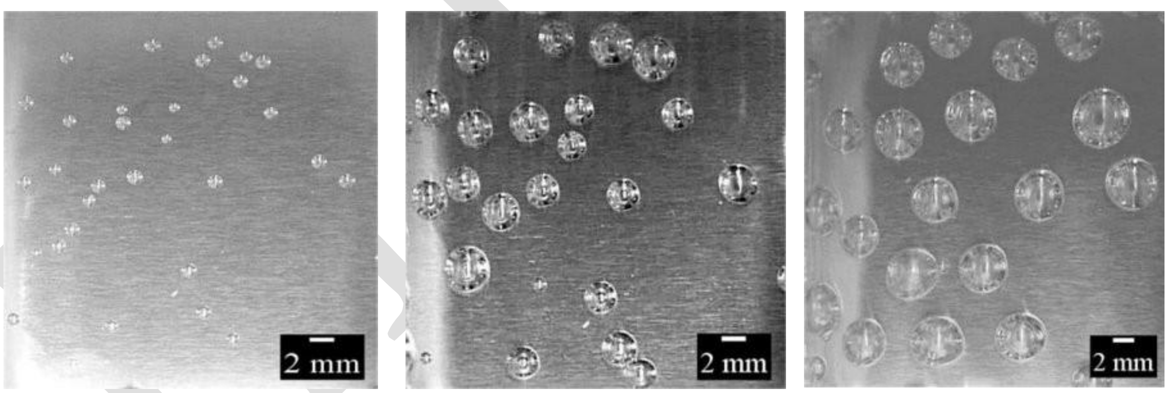

a) ***t* = 5 min**
Øb=0.836 ± 0.091mm

b) ***t* = 15 min**
Øb=2.287 ± 0.161mm

c) ***t* = 30 min**
Øb=3.332± 0.164mm

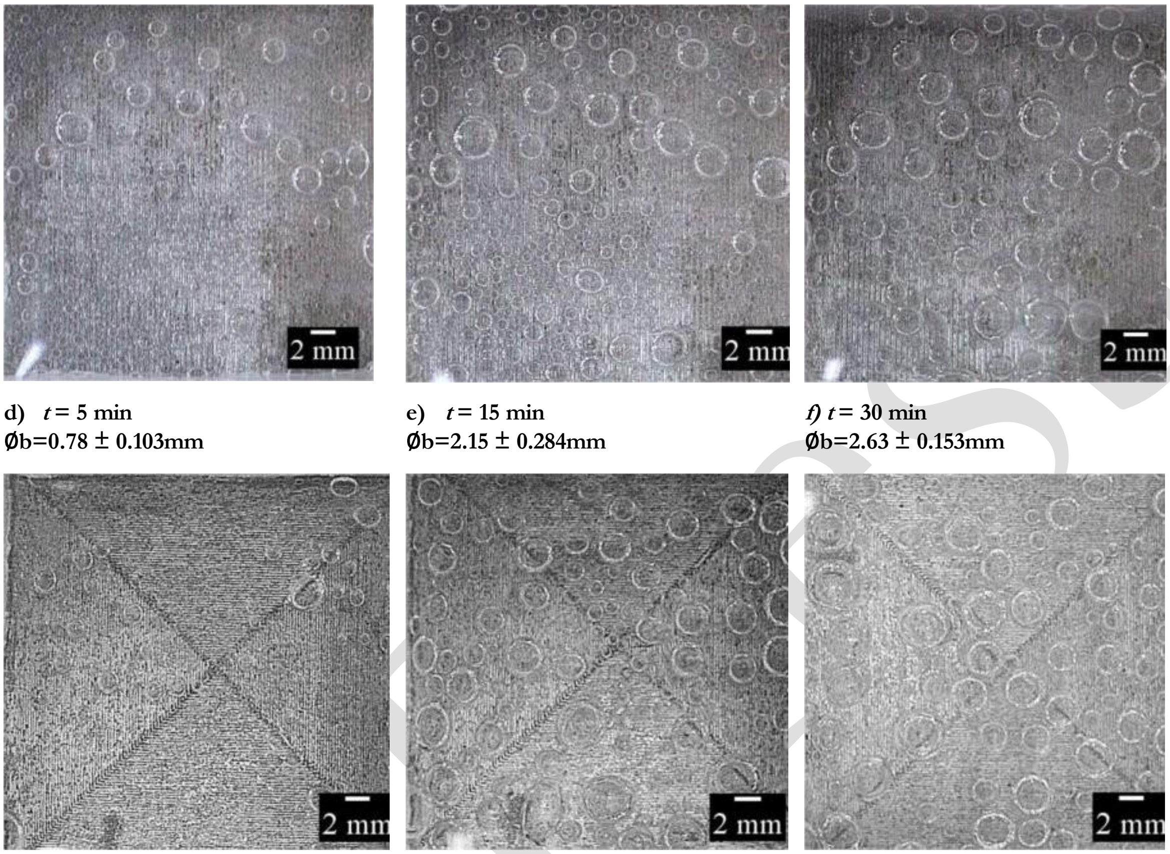

d) ***t*** **= 5 min**
Øb=0.78 ± 0.103mm

e) ***t*** **= 15 min**
Øb=2.15 ± 0.284mm

f) ***t*** **= 30 min**
Øb=2.63 ± 0.153mm

g) ***t*** **= 5 min**
Øb=0.675 ± 0.206mm

h) ***t*** **= 15 min**
Øb=1.569 ± 0.285mm

i) ***t*** **= 30 min**
Øb=2.240 ± 0.284mm

Figure 8. Evolution of bubbles during heating by Peltier effect of the different surfaces. Smooth surface (**a-c**), Vertical surface (**d-f**) and (**g-i**) square surface.

The changes in the average bubble diameter are shown in (**Figure 9)**. The smooth surface produced the largest average bubble diameter, followed by the vertical surface and the square surface respectively, the bubbles do not form instantaneously, suggesting that a minimum amount of thermal energy is required to be transferred to the liquid before the bubble nuclei can reach an optimal detachment size. In this sense, the bubbles formed in the shortest time on the smooth surface, followed by the surface with a vertical pattern and the surface with a square pattern. In all cases, the growth of the bubble follows a logarithmic behavior reaching a maximum size between 15 and 20 minutes (900 and 1200 s) depending on the type of surface. The study shows that there comes a time when regardless of the constant heat flow supplied by the Peltier cell, the bubble stops growing, the largest bubble size (3.33 mm) corresponds to the smooth surface followed by the vertical surfaces. (2.63 mm) and square surface (2.24 mm).

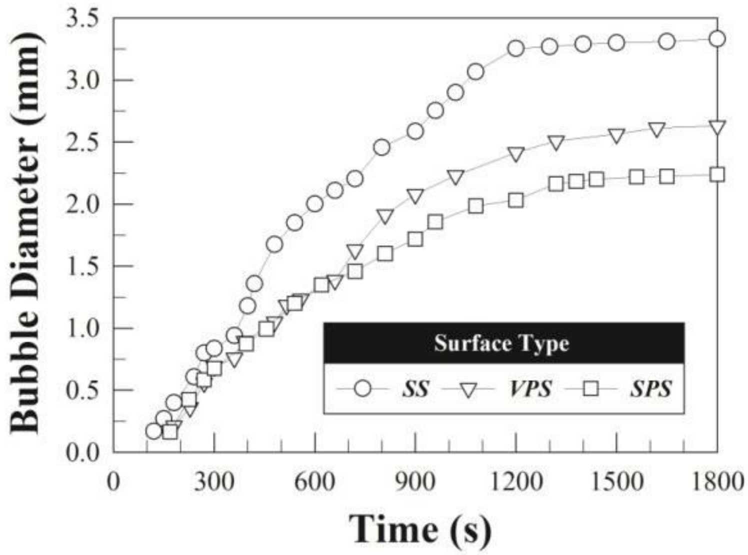

Figure 9. Average bubble diameter as a function of time for the three surface types.

Active Nucleation sites and Bubble Detachment Frequency

Active nucleation sites are overheated points that generate bubbles, if a bubble grows up to a certain size and generates enough inside pressure it will leave the surface; otherwise, it will collapse. According to (**Figure 8**), it was observed that the SS surface showed the least generation of bubbles and the largest bubble diameter, with two or more bubbles coalescing on the surface.

Also, larger bubbles were observed leaving the surface in comparison with the micro-milled surfaces which generate more bubbles of smaller size. The latter is a consequence of many bubbles that nucleate on the valleys and peaks of the micro-milled surface, with the sharp corners of the mini fins acting as nucleation sites. The depth of the micro-milled surface (the measured roughness values were 75.86 and 74.16 μm for the VPS and SPS surfaces, respectively, and 1.89 μm for the SS surface) promotes more nucleation sites; the ratio of nucleation sites on the SPS surface to that of the SS surface was approximately 3.

The bubble detachment frequency was estimated to complete the analysis of bubble dynamics. The analysis was carried out when the system was in a stable state (15-30 min), that is, the boiling nucleated remained constant, five random minutes were taken during this time, the formation and detachment of individual bubbles was tracked, obtaining an average for the frequency of bubble detachment for three different experiments (**Table 3**). The tracking of the bubble was carried out in the Tracker software (22), which allows the video playback to be slowed down, allowing the counting to be carried out more efficiently.

Table 3. Number of nucleation sites (N) and bubble detachment frequency (fb)

Surface Type	N	f_b
SS	28	49
VPS	77	66
SPS	81	90

Video recordings taken during experiments with the SS surface showed that bubble detachment was slow, staying approximately constant most of the time. The SPS surface increment 2:1 the frequency of bubble detachment concerning the SS-type surface, resulting in a minimum diameter of bubble detachment it is worth noting that during the tests with the SPS surface, few bubbles collapsed before detachment, due to the hydrostatic pressure.

Heat Extraction

The resulting macroscopic heat balance equation presented in the methodology (Eq. 2) was used to estimate the transferred heat from the surfaces to the liquid pool. Since the heat balance used the measured thermal response at a position in the liquid pool, the estimated heat flux represents the amount transferred to the liquid pool without considering the heat removed by the bubbles, however, the impact of the generation and detachment of bubbles can be seen in the values obtained for the coefficient of heat extraction (h). **Figure 10** shows the estimated convection coefficient as a function of time for the three surfaces studied. It can be seen that the smooth surface results in the least amount of heat extraction by the system, since this case presents the highest heating of the water in the pool but at the same time the surface has fewer sites of nucleation and low detachment of bubbles, reaching a maximum value of 5.4 W cm^{-2} K^{-1}; after that the heat flux remains constant, so the system is said to reach a steady state. The vertical micro-milled surface shows a maximum heat flux of approximately 7.7 W cm^{-2} K^{-1} and the square surface presents the highest value of 11.45 W cm^{-2} K^{-1}; values reached after 15 minutes of experimentation, time in which the system remains in constant boiling, generating the same diameter of detachment bubble.

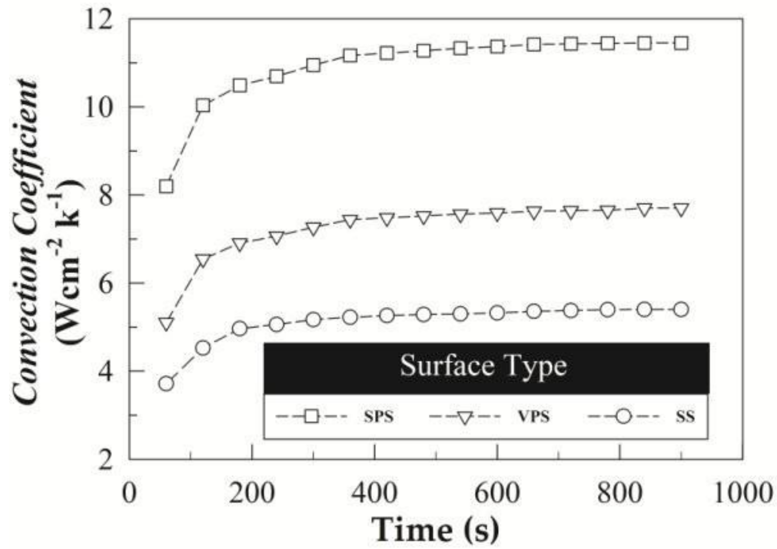

Figure 10. Convection coefficient as a function of time.

The experimental findings (**Table 4**) support the initial hypothesis that micropatterning enhances control over nucleate boiling and improves heat dissipation. Compared to smooth surfaces, the micropatterned samples exhibited greater heat transfer areas, surface roughness, and increased bubble detachment frequencies, this contributes to more efficient boiling heat transfer. Furthermore, these surfaces also demonstrated lower surface temperatures and smaller bubble diameters, indicating that the enhanced nucleation site density promotes rapid bubble release and effective thermal regulation. Although the convection coefficients varied across surface types, the overall trend confirms that micropatterning optimizes bubble dynamics and heat extraction. These results validate the proposed mechanism, showing that surface roughness and exposed transfer area can simultaneously increase nucleation activity and stabilize boiling performance.

Table 4. Comparative Results of Micropatterned Surfaces in Nucleate Boiling

Surface Type	Heat Transfer Area	Average Roughness	Surface Temperature	Bubble Diameter	Nucleation Sites	Detachment Frequency	Convection Coefficient
	(m^2)	(μm)	(K)	(mm)	(-)	(min^{-1})	($W\ cm^{-2}\ K^{-1}$)
SS	9.0×10^{-4}	1.89	384	3.32	28	49	5.40
VPS	1.4×10^{-3}	75.86	380	2.63	77	66	7.70
SPS	2.5×10^{-3}	74.16	377	2.24	81	90	11.45

DISCUSSION

Micromachining is a technique used in recent years that allows the creation of microscales structures and patterns on metal surfaces. Microscale patterns and structures increase the possibility of “control” over bubble formation sites and heat extraction. The proposal to implement new and novel geometric patterns to evaluate the boiling pool phenomenon has demonstrated an increase in heat extraction due to the rise in nucleation sites, growth, and bubble detachment during the boiling when micromachined surfaces are used compared to smooth surfaces [(23)].

It is usual to carry out micromachining in the order of millimeters but in the scale of nanometers it is less observed in literature. The geometric of micropatterns can influence surface thermal profiles during the heating [(24)], this is difficult to find in the literature and allows the opportunity to generate future research.

During pool boiling, a constant supply of fresh liquid to the heated surface facilitates cooling of the exposed surface. From the results it is inferred that the flow towards the liquid/solid interface of the smooth type of surface is obstructed by the low rate of bubble detachment, making it difficult for new bubbles to form and, therefore, making it difficult to extract heat from through the formation of bubbles, so it is inefficient. The micromachined surface promotes the nucleation of a higher number of bubbles concerning the smooth surface because there is overheating in the valleys [(25)], which causes early nucleation of bubbles; the bubbles are smaller and separate from the surface faster compared to the smooth surface, the experimentation of dynamics of the bubbles showed that there is a lateral coalescence between the bubbles for all surfaces [(26)].

The heat flux calculated for the micromachined surfaces is the highest due to the nucleation, growth, and detachment of bubbles considered. The heat loss is due to the generation of smaller bubbles, and the heat transferred by the surface to the liquid pool. Roughness is a factor manipulated to have greater control over the generation of bubbles, and the pattern geometry can interfere with the phenomenon of flow instability in nucleate boiling [27].

Micromachining news designs are available to be implemented in high-power electronic heatsinks. The trend of electronic components towards miniaturization requires higher energy and more efficient methods for heat extraction[28]. The micromachining on metal surfaces represents a powerful tool for the study and improvement of boiling heat transfer. Its ability to create precise and controlled structures at the microscale opens new possibilities in the design of more efficient and effective cooling systems.

This investigation was carried out at the micrometer scale under controlled thermal conditions, which imposes certain restrictions in the analysis. Specifically, experimental design makes it difficult to extend the results to mathematical simulations that incorporate phase change phenomena. In addition, the setup was constrained to a controlled-pressure system, limiting the ability to vary saturation conditions of the liquid and, consequently, the nucleate pool boiling behavior. Even with these limitations, the findings provide valuable insights into microscale heat transfer and highlight the need for further studies that explore broader operating conditions and advanced modeling approaches.

CONCLUSIONS

Surface micropatterning significantly enhanced boiling heat transfer by promoting a more homogeneous distribution of nucleation sites, increasing bubble detachment frequency, and improving heat extraction. The use of a Peltier cell as the heating source strengthened the experimental approach by minimizing thermal inertia effects associated with conventional resistive heating and ensuring a uniform heat flux. Micropatterned surfaces produced up to three times more nucleation sites than smooth surfaces, while bubble detachment frequency nearly doubled for micro-finned surfaces with a relative roughness of approximately 75 μm. These effects were reflected in higher convection coefficients, reaching 11.45 $W/cm^2 \cdot K$ for square patterns, compared with 7.7 $W/cm^2 \cdot K$ for vertical patterns and 5.4 $W/cm^2 \cdot K$ for smooth surfaces. In addition, micropatterned surfaces exhibited lower surface temperatures and smaller bubble diameters, confirming their enhanced thermal performance. Overall, these results suggest that engineered roughness and increased heat transfer area represent promising strategies for optimizing boiling dynamics, providing a potential pathway toward advanced thermal management in liquid cooling systems. Future work should extend this approach to nanoscale surface engineering to further improve cooling performance in high-power electronic applications.

ETHICAL CONSIDERATIONS

This study did not involve human participants, animals, biological materials, or personal data; therefore, ethics committee approval and informed consent were not applicable. The experimental work was carried out in accordance with institutional laboratory safety procedures and standard engineering research practices.

FINANCIAL SUPPORT

The authors thank the support of project No. 14332.22-P of TecNM. National Council of Humanities, Sciences, and Technologies (CONNECT) of Mexico for postgraduate scholarship No. 473107.

CONFLICTS OF INTEREST

The authors declare that they have no conflict of interest.

REFERENCES

1. **Paruya S, Bhati J, Akhtar F.** Numerical model of bubble shape and departure in nucleate pool boiling. Int J Heat Mass Transf [Internet]. 2021;180:121756. http://dx.doi.org/10.1016/j.ijheatmasstransfer.2021.121756

2. **Wang Y, Cai J.** Numerical investigation on bubble evolution during nucleate boiling using diffuse interface method. Int J Heat Mass Transf [Internet]. 2017;112:28–38. http://dx.doi.org/10.1016/j.ijheatmasstransfer.2017.04.109

3. **Wei J, Liu Z, Gong S, Cheng P.** Effects of contact angle hysteresis on nucleate boiling bubble dynamics and heat transfer. Int J Heat Mass Transf [Internet]. 2026;256:128122. http://dx.doi.org/10.1016/j.ijheatmasstransfer.2025.128122

4. **Yu CK, Lu DC.** Pool boiling heat transfer on horizontal rectangular fin array in saturated FC-72. Int J Heat Mass Transf [Internet]. 2007;50(17–18):3624–37. http://dx.doi.org/10.1016/j.ijheatmasstransfer.2007.02.003

5. **Ghazivini M, Hafez M, Ratanpara A, Kim M.** A review on correlations of bubble growth mechanisms and bubble dynamics parameters in nucleate boiling. J Therm Anal Calorim [Internet]. 2022;147(11):6035–71. http://dx.doi.org/10.1007/s10973-021- 10876-2

6. **Zhou P, Huang R, Huang S, Zhang Y, Rao X.** Experimental investigation on active nucleation site density and bubble departure frequency in subcooled flow boiling by using bubble tracking algorithm. Int

J Heat Mass Transf [Internet]. 2020;148:119081. http://dx.doi.org/10.1016/j.ijheatmasstransfer.2019.119081

7. **Vodopivec M, Berhe MG, Bucci M, Zupančič M, Fontanarosa D, Može M,** et al. Experimental investigation of the impact of surface tension and artificial nucleation site geometry on the bubble growth. J Phys Conf Ser [Internet]. 2024;2766(1):012117. http://dx.doi.org/10.1088/1742-6596/2766/1/012117

8. **Gong S, Cheng P.** Lattice Boltzmann simulations for surface wettability effects in saturated pool boiling heat transfer. Int J Heat Mass Transf [Internet]. 2015;85:635–46. http://dx.doi.org/10.1016/j.ijheatmasstransfer.2015.02.008

9. **Kadivar M, Tormey D, McGranaghan G.** CFD of roughness effects on laminar heat transfer applied to additive manufactured minichannels. Heat Mass Transf [Internet]. 2024;60(12):1915–29. http://dx.doi.org/10.1007/s00231-022-03268-1

10. **Jones BJ, McHale JP, Garimella SV.** The influence of surface roughness on nucleate pool boiling heat transfer. J Heat Transfer [Internet]. 2009;131(12):121009. http://dx.doi.org/10.1115/1.3220144

11. **McHale JP, Garimella SV.** Bubble nucleation characteristics in pool boiling of a wetting liquid on smooth and rough surfaces. Int J Multiph Flow [Internet]. 2010;36(4):249–60. http://dx.doi.org/10.1016/j.ijmultiphaseflow.2009.12.004

12. **Wilson ME, Kota N, Kim Y, Wang Y, Stolz DB, LeDuc PR,** et al. Fabrication of circular microfluidic channels by combining mechanical micromilling and soft lithography. Lab Chip [Internet]. 2011;11(8):1550–5. http://dx.doi.org/10.1039/c0lc00561d

13. **Cheng Y, Xu J, Sui Y.** Numerical study on drag reduction and heat transfer enhancement in microchannels with superhydrophobic surfaces for electronic cooling. Appl Therm Eng [Internet].2015;88:71–81. http://dx.doi.org/10.1016/j.applthermaleng.2014.10.058

14. **Wang J, Shen W-J, Ma J-C, Wang J, Zhao W-D, Shi Y-X.** Flow distribution regulation in microchannels for emitter side-mounted ionic wind heat sink and its implication for high- efficiency thermal management. Int J Heat Mass Transf [Internet]. 2025;249:127245. http://dx.doi.org/10.1016/j.ijheatmasstransfer.2025.127245

15. **Jaikumar A, Kandlikar SG.** Enhanced pool boiling heat transfer mechanisms for selectively sintered open microchannels. Int J Heat Mass Transf [Internet]. 2015;88:652–61. http://dx.doi.org/10.1016/j.ijheatmasstransfer.2015.04.100

16. **Huang G, Li W, Ma J, Ren C, Li C.** High-frequency alternating nucleate boiling of water enabled by microslot arrays in microchannels. Int J Heat Mass Transf [Internet].2020;150:119271. http://dx.doi.org/10.1016/j.ijheatmasstransfer.2019.119271

17. **Sato Y, Niceno B.** Nucleate pool boiling simulations using the interface tracking method: Boiling regime from discrete bubble to vapor mushroom region. Int J Heat Mass Transf [Internet]. 2017;105:505–24. http://dx.doi.org/10.1016/j.ijheatmasstransfer.2016.10.018

18. **Kurnia JC, Sasmito AP, Mujumdar AS.** Numerical investigation of laminar heat transfer performance of various cooling channel designs. Appl Therm Eng [Internet]. 2011;31(6– 7):1293–304. http://dx.doi.org/10.1016/j.applthermaleng.2010.12.036

19. **Urbano A, Tanguy S, Huber G, Colin C.** Direct numerical simulation of nucleate boiling in micro-layer regime. Int J Heat Mass Transf [Internet]. 2018;123:1128–37. http://dx.doi.org/10.1016/j.ijheatmasstransfer.2018.02.104

20. **Ahmadi S, Hanafizadeh P, Eraghubi M, Robinson AJ.** Upward flow boiling of HFE- 7000 in high frequency AC electric fields. International Journal of Thermofluids [Internet]. 2021;10:100076. http://dx.doi.org/10.1016/j.ijft.2021.100076

21. **Kweon YC, Kim MH.** Experimental study on nucleate boiling enhancement and bubble dynamic behavior in saturated pool boiling using a nonuniform dc electric field. Int J Multiph Flow [Internet]. 2000;26(8):1351–68. https://doi.org/10.1016/S0301-9322(99)00090-7

22. **Tracker video analysis and modeling tool for physics education** [Internet]. Github.io. [cited 2026 April 17]. Available from: https://opensourcephysics.github.io/tracker-website/

23. **Al-Nagdy AA, Khalaf-Allah RA, Mohamed SM, Saeed E, Abdelaziz GB.** Pool boiling performance enhancement via latest microstructural surface modifications: a review. J Therm Anal Calorim [Internet]. 2025;150(25):20481–515. http://dx.doi.org/10.1007/s10973-025-14915-0

24. **Hożejowska S, Kaniowski R, Pastuszko R.** Application of the Trefftz method for pool boiling heat transfer on open microchannel surfaces. Heat Trans Eng [Internet]. 2022;43(3– 5):362–70. Available from: http://dx.doi.org/10.1080/01457632.2021.1874669

25. **Prakash S, Yeom J.** Nanofluidics and Microfluidics: Systems and Applications. Norwich, CT, Estados Unidos de América: William Andrew Publishing; 2017.

26. **Sarode A, Raj R, Bhargav A.** Scalable macroscale wettability patterns for pool boiling heat transfer enhancement. Heat Mass Transf [Internet]. 2020;56(3):989–1000. http://dx.doi.org/10.1007/s00231-019-02783-y

27. **Liu Z, Yao X, Cheng X, Wu H, Wang H, Shen H.** Experimental study on two-phase boiling in wavy copper microchannels fabricated with ultrafast laser micromachining. J Micromech Microeng [Internet]. 2020;30(6):065011. http://dx.doi.org/10.1088/1361-6439/ab870b

28. **Dinis H, Mendes PM.** A comprehensive review of powering methods used in state-of-the- art miniaturized implantable electronic devices. Biosens Bioelectron [Internet]. 2021; 172:112781. http://dx.doi.org/10.1016/j.bios.2020.112781